Massless Links with External Forces and Bushing Effect for Multibody Dynamic Analysis

Jeong-Hyun Sohn*
Graduate school, Pusan National University, Pusan 609-735, Korea
Wan-Suk Yoo, Keum-Shik Hong
School of Mechanical Engineering, Pusan National University, Pusan 609-735, Korea
Kwang-Suk Kim
Department of Automobile Engineering, Inha Technical College, Inchon

When the contribution of lightweight components to the total energy of a system is small, the inertia effects are sometimes ignored by replacing them to massless links. For example, a revolute-spherical massless link generates two kinematic constraint equations between adjacent bodies and allows four relative degrees of freedom. In this paper, to implement a massless link systematically in a computer program using the velocity transformation technique, the velocity transformation matrix of massless links is derived and numerically implemented. The velocity transformation matrix for a revolute-spherical massless link and a revolute-universal massless link are appeared as a 6×4 matrix and a 6×3 matrix, respectively. A massless link model in a suspension composite joint transmitting external forces is also developed and the numerical efficiency of the proposed model is compared to a conventional multibody model. For a massless link transmitting external forces, forces acting on links are resolved and transmitted to the attached points with a quasi-static assumption. Numerical examples are presented to verify the formulation.

Key Words : Multi-body Dynamics, Massless Link, Velocity Transformation Technique, Simulation

1. Introduction

With the help of high performance of computers, multi-body dynamic analysis technique has become one of the most effective tools in the machine and automobile industries. Several commercial programs such as DADS and ADAMS, which are available in the computer-aided analysis for multi-body systems, have been developed and widely used. (CADSI, 1995; M. D. I, 1994)

* Corresponding Author,
E-mail : jhson@mail.metric.or.kr
TEL : +82-51-510-1457; **FAX** : +82-51-512-9835
Department of Mechanical Enginerring, Pusan National University, Jangjun-dong, Keumjung-ku, Pusan 609-735, Korea. (Manuscript **Received** August 17, 2001; **Revised** February 27, 2002)

In a multi-body dynamic analysis, the equations of the motion are derived based on masses of components, kinematic constraints, and force elements such as springs, dampers and actuators. Among the major components in a system, the mass of one component may be comparatively smaller than others. When a large force is applied to the small mass component, the equations of motion of the overall system may be ill-conditioned and thus the numerical efficiency of the computer simulation is seriously decreased. To overcome this numerical inefficiency, many researchers have used composite joints to model a small mass component. (Haug, 1989; Nikravesh, 1988) To improve the numerical efficiency in vehicle dynamic analysis, Kading and Vanderploeg(1985) derived a solid axle suspension super-element to apply to the front and rear suspension

in a vehicle dynamic analysis. McCullough and Haug(1986) derived the suspension of a track vehicle from a composite joint and carried out the dynamic analysis.

In these modeling techniques, small mass components are replaced to massless links and equivalent kinematic constraints. However, these modeling techniques could not handle a massless link transmitting force elements, which often appear in the lower control arm of a McPherson or a Double-Wishbone suspension.

In this paper, to implement a massless link concept in a computer program using the velocity transformation technique, the velocity transformation matrix of a massless link is derived and numerically implemented. And a new modeling technique for a massless link transmitting external forces is suggested. The computer program AutoDyn7 (Kim et al, 1999) used in this paper employs the velocity transformation technique (Nikravesh, Gim, 1993; Kim, Vanderploeg, 1986; Lee et al., 1993). The kinematic relation and constraint equations of a massless link in Cartesian coordinates are well explained in references. (Haug, 1989; Nikravesh, 1988) Although the kinematic relation of a massless link can be treated as constraint equations in the equation of motion using velocity transformation technique, the derivation of velocity transformation matrix of a massless link may be systematic and much convenient. The efficiency of the proposed method is confirmed through several simulations, four-bar mechanism and the vehicle.

In section 2, the velocity transformation matrix of massless links is derived and numerically implemented in the AutoDyn7 program. In section 3, the massless link with external force elements is considered. Numerical examples are suggested in section 4. The efficiency of the proposed model is compared to a rigid body model with mass effect. The conclusions of this paper are presented in section 5.

2. Derivation of Velocity Transformation Matrix of Massless Links

2.1 Equations of Motion Using Velocity Transformation Techniques

The velocity transformation method is proposed to obtain the generality of Cartesian coordinates and the numerical efficiency in joint coordinates. This method employs a graph theory to analyze the topology of a system. As a result of topology analysis, a tree structure and a path matrix of the system are made to show the connectivity of bodies from the base body to the end body. The connectivity is defined from the types of joints between the bodies. The velocity transformation matrix of a system can be formed by putting block matrix to proper position according to the path matrix. This block matrix imposes velocity contribution of each joint to the velocity of each body. When the velocity transformation matrix is formed, the equations of motion can be converted from Cartesian coordinate space to joint coordinate space. This method confirms both the numerical efficiency and the generality of equations of motion.

Let's consider the constraint equations in joint coordinates as followings:

$$\boldsymbol{\Phi}(\mathbf{q}, t)=0 \tag{1}$$

where $\mathbf{q}$ is the vector of joint coordinates.

The time derivative of Eq. (1) is written as:

$$\boldsymbol{\Phi}_{\mathrm{q}}\dot{\mathbf{q}}+\boldsymbol{\Phi}_{t}=0 \tag{2}$$

And the time derivative of Eq. (2) is written as:

$$\boldsymbol{\Phi}_{\mathrm{q}}\ddot{\mathbf{q}}=\bar{\boldsymbol{\gamma}} \tag{3}$$

$$\bar{\gamma}=[(\boldsymbol{\Phi}_{\mathrm{q}}\dot{\mathbf{q}})_{\mathrm{q}}\dot{\mathbf{q}}+2\boldsymbol{\Phi}_{\mathrm{q}t}\dot{\mathbf{q}}+\boldsymbol{\Phi}_{tt}] \tag{4}$$

where $\boldsymbol{\Phi}_{\mathrm{q}}$ means the Jacobian matrix of the constraint equations. Using the velocity transformation matrix and Lagrange multiplier $\bar{\boldsymbol{\lambda}}$, the equations of motion are written as:

$$\bar{\mathbf{M}}\ddot{\mathbf{q}}+\boldsymbol{\Phi}_{\mathrm{q}}{}^{T}\bar{\boldsymbol{\lambda}}=\bar{\mathbf{g}} \tag{5}$$

where $\bar{\mathbf{M}}=\mathbf{B}^{T}\mathbf{M}\mathbf{B}$ is the generalized mass matrix, $\Phi_{q}=\Phi_{y}B$ gives an easy calculation of Jacobian matrix in joint coordinates, $\bar{\mathbf{g}}=\mathbf{B}^{T}[\mathbf{g}-\mathbf{M}\dot{\mathbf{B}}\dot{\mathbf{q}}-\mathbf{M}\mathbf{B}\dot{\mathbf{q}}]$ is the generalized force vector. By com-

bining Eq. (3) and Eq. (5), the equations of motion are written in the matrix form as:

$$\begin{bmatrix} \bar{\mathbf{M}} & \boldsymbol{\Phi}_{\mathbf{q}}{}^{T} \\ \boldsymbol{\Phi}_{\mathbf{q}} & 0 \end{bmatrix} \begin{bmatrix} \ddot{\mathbf{q}} \\ \bar{\lambda} \end{bmatrix} = \begin{bmatrix} \bar{\mathbf{g}} \\ \bar{\gamma} \end{bmatrix} \tag{6}$$

2.2 Velocity Transformation Matrix of RSML

Fig. 1 shows the configuration of a revolute-spherical massless link. In Fig. 1, R and S represent the revolute joint definition point and the spherical joint definition points, respectively. The massless link is connected to the reference body j with a revolute joint and to the adjacent body i with a spherical joint. Figure 2 shows the coordinate system of a revolute-spherical massless link.

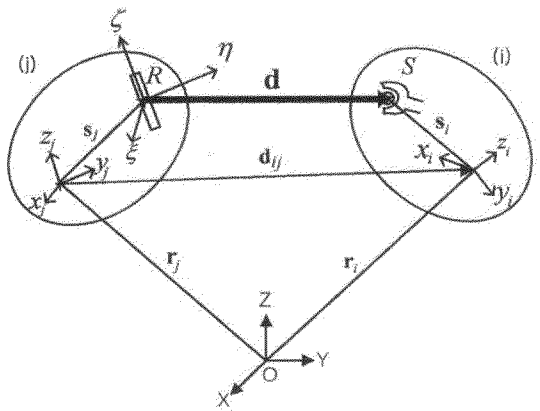

Fig. 1 Configuration of a RSML

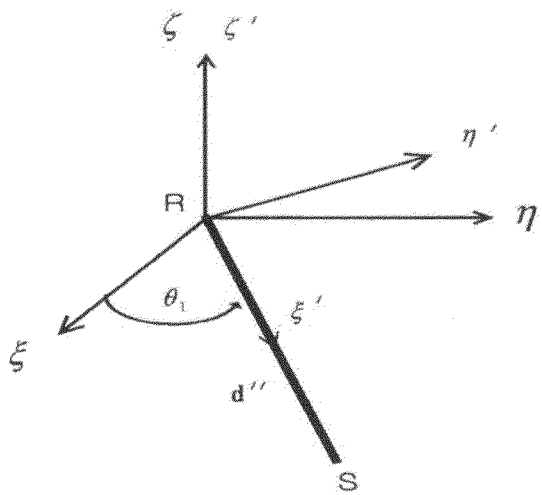

Fig. 2 Coordinate system of a RSML

In Fig. 2, $\xi\eta\zeta$ coordinate system is coordinate system fixed at the revolute joint of the reference body j and the ζ axis represents the rotational axis of the revolute joint. The $\xi'\eta'\zeta'$ coordinate system is a coordinate system rotated from the $\xi n\zeta$ coordinate about ζ axis.

The vector $\mathbf{d}''$ connecting between point R and point S represents a massless link of length l, which is defined at the $\xi'\eta'\zeta'$ coordinate system. The position vector to the origin of the local coordinate system of body i can be written as:

$$\mathbf{r}_i = \mathbf{r}_j + \mathbf{s}_j + \mathbf{d} - \mathbf{s}_i \tag{7}$$

where $\mathbf{r}_i$ and $\mathbf{r}_j$ are a vector from the inertial reference frame to the origin of the body i and body j, respectively. $\mathbf{s}_j$ is a vector from the origin of the body j to the revolute joint definition point and $\mathbf{s}_i$ is a vector from the origin of the body i to the spherical joint definition point. The vector $\mathbf{d}$ is defined from the revolute joint definition point (R) of body j to the spherical joint definition point (S) of body i, which may not be perpendicular to the revolute joint axis. These vectors are defined in the inertial reference frame (XYZ).

Vector $\mathbf{d}''$ can be defined from the initial joint definition point of input data as follows:

$$\mathbf{d}_0 = \mathbf{A}_{j0}\mathbf{A}_{rj}\mathbf{A}_{\theta_1}\mathbf{d}'' \tag{8}$$

where $\mathbf{d}_0$ is the initial position vector from the revolute joint definition point of body j to the spherical joint definition point of body i. The matrix $\mathbf{A}_{j0}$ is a coordinate transformation matrix from the local coordinate system of body j to the global coordinate system at initial state. The matrix $\mathbf{A}_{rj}$ is a coordinate transformation matrix from the revolute joint coordinate system of body j to the local coordinate system of body j at the initial state, which is a constant matrix. The matrix $\mathbf{A}_{\theta_1}$ is a rotation matrix due to the revolute joint rotation.

Considering the rotation of the revolute joint is zero at the initial state, $\theta_1=0$, the vector $\mathbf{d}''$ is calculated from Eq. (8) as followings:

$$\mathbf{d}'' = (\mathbf{A}_{j0}\mathbf{A}_{rj})^{T}\mathbf{d}_0 \tag{9}$$

The vector $\mathbf{d}$ can be calculated from $\mathbf{d}''$ as followings:

$$\mathbf{d}=\mathbf{A}_j\mathbf{A}_{\gamma j}\mathbf{A}_{\theta_1}\mathbf{d}'' \tag{10}$$

The translational velocity vector at the origin of the local coordinate system of body may be written as:

$$\dot{\mathbf{r}}_i=\dot{\mathbf{r}}_j+\dot{\mathbf{s}}_j+\dot{\mathbf{d}}-\dot{\mathbf{s}}_i \tag{11}$$

where $(\dot{})$ represents the time derivative. The velocity vector $\dot{\mathbf{d}}$ of RSML is calculated as:

$$\begin{aligned}\dot{\mathbf{d}}&=\tilde{\boldsymbol{\omega}}_j\mathbf{d}+\mathbf{A}_j\mathbf{A}_{\gamma j}\dot{\mathbf{A}}_{\theta_1}\mathbf{d}''\\&=\tilde{\boldsymbol{\omega}}_j\mathbf{d}+\mathbf{A}_j\mathbf{A}_{\gamma j}\dot{\theta}\tilde{\mathbf{u}}_1'\mathbf{A}_{\theta_1}\mathbf{d}''\\&=\tilde{\boldsymbol{\omega}}_j\mathbf{d}+\dot{\theta}_1\tilde{\mathbf{u}}_1\mathbf{d}\end{aligned} \tag{12}$$

where $\boldsymbol{\omega}_j$ is the angular velocity vector of body j. The skew-symmetric matrix $\tilde{\boldsymbol{\omega}}_j$ is defined as $\tilde{\boldsymbol{\omega}}_j\mathbf{a}=\boldsymbol{\omega}_j\times\mathbf{a}$. The vectors $\mathbf{u}_1'$ and $\mathbf{u}_1$ represent unit vectors along the revolute joint axes in $\xi'\eta'\zeta'$ coordinate system and the inertial reference frame (XYZ), respectively.

The terms $\dot{\mathbf{s}}_j$ and $\dot{\mathbf{s}}_i$ in Eq. (11) are also calculated as:

$$\dot{\mathbf{s}}_j=\tilde{\boldsymbol{\omega}}_j\mathbf{s}_j \tag{13}$$

$$\dot{\mathbf{s}}_i=\tilde{\boldsymbol{\omega}}_i\mathbf{s}_i=\tilde{\mathbf{s}}_i\boldsymbol{\omega}_i \tag{14}$$

The angular velocity of the body i is written as:

$$\boldsymbol{\omega}_i=\boldsymbol{\omega}_j+\dot{\theta}_1\mathbf{u}_1+\dot{\theta}_2\mathbf{u}_2+\dot{\theta}_3\mathbf{u}_3+\dot{\theta}_4\mathbf{u}_4 \tag{15}$$

where $\dot{\theta}_1$ means the angular velocity of the revolute joint. And $\dot{\theta}_2$, $\dot{\theta}_3$, and $\dot{\theta}_4$ represent the angular velocity of the spherical joint, respectively. The vector $\mathbf{u}_2$, $\mathbf{u}_3$, and $\mathbf{u}_4$ represent unit vectors along the joint axes of the spherical joint, respectively.

Inserting Eqs. (12~15) into Eq. (11) yields:

$$\begin{aligned}\dot{\mathbf{r}}_i=\dot{\mathbf{r}}_j+\tilde{\boldsymbol{\omega}}_j(\mathbf{s}_j+\mathbf{d}-\mathbf{s}_i)+\dot{\theta}_1(\tilde{\mathbf{u}}_1\mathbf{d}+\tilde{\mathbf{s}}_i\mathbf{u}_1)\\+\tilde{\mathbf{s}}_i(\dot{\theta}_2\mathbf{u}_2+\dot{\theta}_3\mathbf{u}_3+\dot{\theta}_4\mathbf{u}_4)\end{aligned} \tag{16}$$

Combining Eq. (15) and Eq. (16), the translational velocity vector and the angular velocity vector of the body i are written in the matrix form as:

$$\begin{bmatrix}\dot{\mathbf{r}}_i\\\boldsymbol{\omega}_i\end{bmatrix}=\begin{bmatrix}\mathbf{I}_3&-\tilde{\mathbf{d}}_{ij}\\\mathbf{0}&\mathbf{I}_3\end{bmatrix}\begin{bmatrix}\dot{\mathbf{r}}_j\\\boldsymbol{\omega}_j\end{bmatrix}+\begin{bmatrix}\tilde{\mathbf{d}}_{ir}\mathbf{u}_1&\tilde{\mathbf{s}}_i\mathbf{u}_2&\tilde{\mathbf{s}}_i\mathbf{u}_3&\tilde{\mathbf{s}}_i\mathbf{u}_4\\\mathbf{u}_1&\mathbf{u}_2&\mathbf{u}_3&\mathbf{u}_4\end{bmatrix}\begin{bmatrix}\dot{\theta}_1\\\dot{\theta}_2\\\dot{\theta}_3\\\dot{\theta}_4\end{bmatrix} \tag{17}$$

where $\mathbf{d}_{ij}=\mathbf{s}_j+\mathbf{d}-\mathbf{s}_i$ and $\mathbf{d}_{ir}=\mathbf{s}_i=\mathbf{d}$. Therefore, the velocity transformation matrix of RSML is written as:

$$\mathbf{B}_{ij}=\begin{bmatrix}\tilde{\mathbf{d}}_{ir}\mathbf{u}_1&\tilde{\mathbf{s}}_i\mathbf{u}_2&\tilde{\mathbf{s}}_i\mathbf{u}_3&\tilde{\mathbf{s}}_i\mathbf{u}_4\\\mathbf{u}_1&\mathbf{u}_2&\mathbf{u}_3&\mathbf{u}_4\end{bmatrix}_{(6\times4)} \tag{18}$$

The time derivative of Eq. (18) is written as:

$$\dot{\mathbf{B}}_{ij}=\begin{bmatrix}\dot{\mathbf{B}}_{11}&\dot{\mathbf{B}}_{12}&\dot{\mathbf{B}}_{13}&\dot{\mathbf{B}}_{14}\\\tilde{\boldsymbol{\omega}}_1\mathbf{u}_1&\tilde{\boldsymbol{\omega}}_2\mathbf{u}_2&\tilde{\boldsymbol{\omega}}_3\mathbf{u}_3&\tilde{\boldsymbol{\omega}}_4\mathbf{u}_4\end{bmatrix}_{(6\times4)} \tag{19}$$

where $\dot{\mathbf{B}}_{11}$, $\dot{\mathbf{B}}_{12}$, $\dot{\mathbf{B}}_{13}$, $\dot{\mathbf{B}}_{14}$ are as followings:

$$\dot{\mathbf{B}}_{11}=\dot{\tilde{\mathbf{d}}}_{ir}\mathbf{u}_1+\tilde{\mathbf{d}}_{ir}\dot{\mathbf{u}}_1 \tag{20}$$

$$\dot{\mathbf{B}}_{12}=\dot{\tilde{\mathbf{s}}}_i\mathbf{u}_2+\tilde{\mathbf{s}}_i\tilde{\boldsymbol{\omega}}_2\mathbf{u}_2 \tag{21}$$

$$\dot{\mathbf{B}}_{13}=\dot{\tilde{\mathbf{s}}}_i\mathbf{u}_3+\tilde{\mathbf{s}}_i\tilde{\boldsymbol{\omega}}_3\mathbf{u}_3 \tag{22}$$

$$\dot{\mathbf{B}}_{14}=\dot{\tilde{\mathbf{s}}}_i\mathbf{u}_4+\tilde{\mathbf{s}}_i\tilde{\boldsymbol{\omega}}_4\mathbf{u}_4 \tag{23}$$

2.3 Velocity Transformation Matrix of RUML

We also derived the velocity transformation matrix for revolute-universal massless link via the same sequence. The velocity transformation matrix and time derivatives of RUML are written as:

$$\mathbf{B}_{ij}=\begin{bmatrix}\tilde{\mathbf{d}}_{ir}\mathbf{u}_1&\tilde{\mathbf{s}}_i\mathbf{u}_2&\tilde{\mathbf{s}}_i\mathbf{u}_3\\\mathbf{u}_1&\mathbf{u}_2&\mathbf{u}_3\end{bmatrix}_{6\times3} \tag{24}$$

$$\dot{\mathbf{B}}_{ij}=\begin{bmatrix}\dot{\mathbf{B}}_{11}&\dot{\mathbf{B}}_{12}&\dot{\mathbf{B}}_{13}\\\tilde{\boldsymbol{\omega}}_1\mathbf{u}_1&\tilde{\boldsymbol{\omega}}_2\mathbf{u}_2&\tilde{\boldsymbol{\omega}}_3\mathbf{u}_3\end{bmatrix}_{6\times3} \tag{25}$$

2.4 Joint Reaction Forces of massless links

Since the mass of a massless link is ignored, joint reaction forces and torques can be calculated by using the equilibrium equations as shown in the Fig. 3.

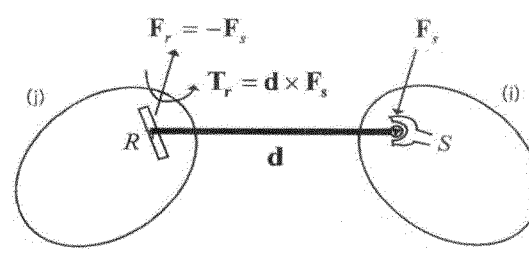

Fig. 3 Joint reaction forces and moments acting on R-S link

3. Massless Link with External Forces

3.1 Force distribution without bushing

When external forces are applied to a massless link, the reaction forces due to the external forces cannot be calculated from using a conventional composite joint. Since the mass of a massless link is small enough compared to masses of other bodies, we assume a quasi-static state. In the quasi-static state, the reaction forces due to a force element can be divided into equivalent forces at attachment points of the massless link. The coordinate of RSML is shown in the Fig. 4 (a). In the Fig. 4(a), L represents the length of a revolute-spherical massless link, a represents the distance from the revolute joint to the external force acting point, and b indicates the distance between the spherical joint and the external force acting point. The R. J and S. J represent the revolute joint and the spherical joint, respectively. Fig. 5 (b) shows all external forces and reaction forces on y-z plane and forces on x-z plane are shown in the Fig. 5(c). Fig. 5 (d) shows the moments along z-axis.

When external forces are applied to a revolute-spherical massless link, three directional forces and two directional moments are found as reaction forces at the revolute joint. Three directional reaction forces are found at the spherical joint. Resultant forces can be divided into the bending direction and the axial direction. In the Fig. 5(a), F_V and T represent the vertical external force and external torque, respectively. F_A and F_B represent the bending direction reaction force at the revolute joint and the spherical joint, respectively. In the Fig. 5(b), F_H represents the axial direction external force. R_A and R_B represent the axial direction reaction force at the revolute joint and the spherical joint, respectively.

The resultant forces on x-z plane are calculated as follows:

$$F_A=\left[\frac{a^2(3L-a)}{2L^3}-1\right]F_v+\frac{3a(2L-a)}{2L^3}T \quad (26)$$

$$F_B=\frac{a^2(a-3L)}{2L^3}F_v+\frac{3a(a-2L)}{2L^3}T \quad (27)$$

$$T_A=\left[\frac{a^2(3L-a)}{2L^2}-a\right]F_v+\frac{3a(2L-a)}{2L^2}T \quad (28)$$

$$R_A=\frac{b}{L}F_h,\ R_B=\frac{a}{L}F_h \quad (29)$$

The resultant forces on y-z plane can be calculated using the same manner as the above. And also, the moments along z-axis can be calculated in the same form as the Eq. (29).

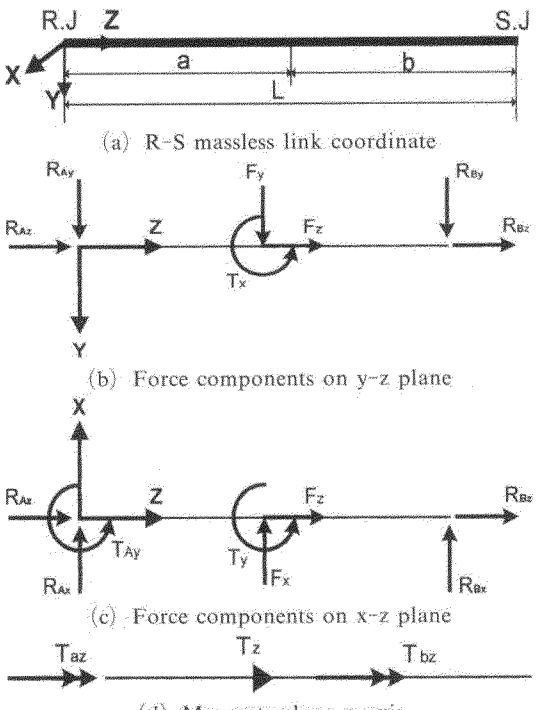

(a) R-S massless link coordinate

(b) Force components on y-z plane

(c) Force components on x-z plane

(d) Moments along z-axis

Fig. 4 Forces and moments acting on R-S link

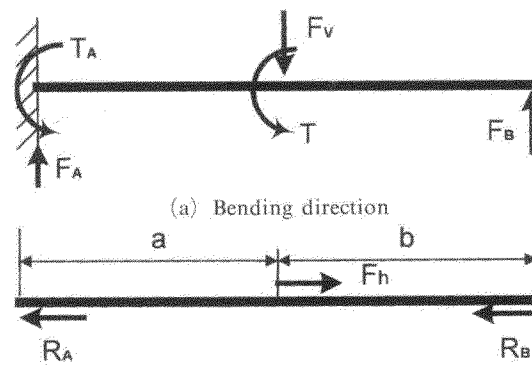

(a) Bending direction

(b) Axial direction

Fig. 5 R-S link reaction force calculation

$$T_{az}=\frac{b}{L}T_z,\ T_{bz}=\frac{a}{L}T_z \tag{30}$$

3.2 Force distribution with bushing

In most vehicle suspension systems, bushing elements are used to improve the ride quality and steering performance. Regulations for bushing elements must be considered in modeling the vehicle suspension system. The joint model, the linear bushing model, and the non-linear bushing model are used to describe the influence of rubber bush compliance on vehicle suspension movement (M. V. Blundell, 1998). The results showed that the bushing element should be included for an accurate modeling of the vehicle systems.

If a bushing element is contained in a lower control arm, it works as a compliant element admitting deformation and damping. Since this bushing element connects adjacent bodies via forces due to bushing deformations, the modeling technique involving the bushing element is quite different from the purely kinematic element.

Fig. 6 shows an example using the bushing-bushing-spherical link with external forces in the vehicle suspension system.

Let us put the deformations of the point B_1 as $\underline{u_1}=[x_1,\ y_1,\ z_1]^T$ and the deformations of the point B_2 as $\underline{u_2}=[x_2,\ y_2,\ z_2]^T$. The potential energy of the lower control arm in the Fig. 5 may be written as follows:

$$V(\underline{u})=\frac{1}{2}\underline{u_1}^T K_1 \underline{u_1}+\frac{1}{2}\underline{u_2}^T K_2 \underline{u_2} \tag{31}$$

where $\underline{u}$ is $[\underline{u_1}^T,\ \underline{u_2}^T]^T$. And K_1 and K_2 are the stiffness matrix of the bushing installed at the point B_1 and B_2, respectively.

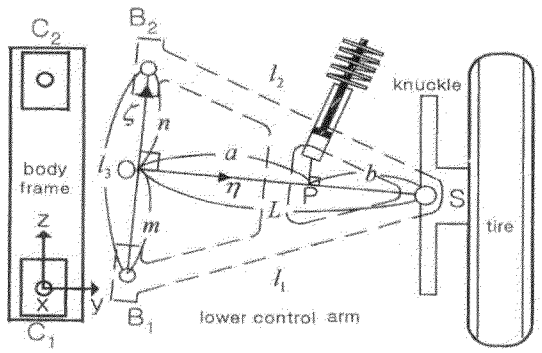

Fig. 6 R-S link with bushing and external force

Even though the bushing is deformed, the length of the lower control arm must remain constant. Thus, the constraints of the bushing-bushing-spherical massless link can be written as follows:

$$\Phi_1=\overline{B_1S}-l_1=0 \tag{32}$$
$$\Phi_2=\overline{B_2S}-l_2=0 \tag{33}$$
$$\Phi_3=\overline{B_1B_2}-l_3=0 \tag{34}$$

The minimizing the potential energy theory is applied to calculate bushing deformations as:

$$\text{Min } V(\underline{u})$$
$$\text{subject to } \Phi_j(\underline{u}),\ j=1,\ 2,\ 3 \tag{35}$$

Then, the overall equation can be reorganized as:

$$f=\min\left[V(\underline{u})+\sum_{j=1}^{3}\lambda_j\Phi_j(\underline{u})\right] \tag{36}$$

where λ_j is the Lagrange multiplier.

Reaction forces at point P can be distributed to equivalent forces and moments at two ends of line O-S, which is a perpendicular line from S to the line B_1-B_2 in Fig. 5. The equivalent forces and moments at point O and point S can be computed by using the elementary beam theory with appropriate boundary conditions. After computing the reaction forces and moments at point O, those are distributed to forces and moments at the two points B_1, B_2. Forces and moments along the line B_1-B_2 can also be calculated by using the beam theory with proper boundary conditions. Detailed process was described at reference (Sohn et al, 2001).

4. Numerical Examples

4.1 Four-bar Mechanism

To confirm the new formulation, such as the velocity transformation matrix of the revolute-spherical massless link and the revolute-universal massless link with external forces, we modeled the four-bar mechanism in two different ways. The first model is the conventional four-bar and the second one has the massless link. Fig. 7 shows the conventional four-bar model. All bodies are assumed rigid bodies. Spherical joint is treated as a cut joint of closed loop system.

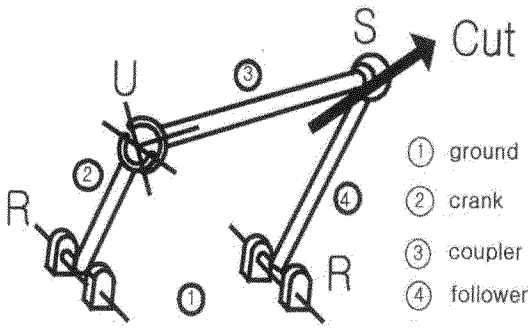

Fig. 7 Conventional four-bar model

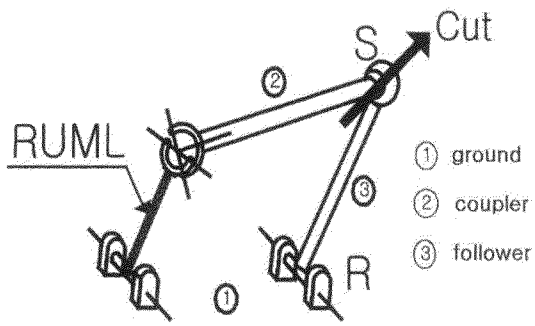

Fig. 8 Four-bar model with a RUML

The velocity transformation matrix in this case is written as;

$$[B]=\begin{bmatrix} \begin{bmatrix}\tilde{u}_1 d_1\\ u_1\end{bmatrix} & 0 & 0 \\ 0 & \begin{bmatrix}\tilde{u}_2 d_2\\ u_2\end{bmatrix} & 0 \\ 0 & \begin{bmatrix}\tilde{u}_2 d_3\\ u_2\end{bmatrix} & \begin{bmatrix}\tilde{u}_3 d_4 & \tilde{u}_4 d_4\\ u_3 & u_4\end{bmatrix} \end{bmatrix}_{18\times 4} \quad (37)$$

Fig. 8 shows the four-bar model with RUML. The crank is a revolute-universal massless link and spherical joint is a cut joint.

The velocity transformation matrix in this case is written as;

$$[B]=\begin{bmatrix} \begin{bmatrix}\tilde{d}_{1r} u_1 & \tilde{s}_i u_2 & \tilde{s}_i u_3\\ u_1 & u_2 & u_3\end{bmatrix} & 0 \\ 0 & \begin{bmatrix}\tilde{u}_4 d_1\\ u_4\end{bmatrix} \end{bmatrix}_{12\times 4} \quad (38)$$

Table 1 represents the comparison of two different cases.

Fig. 9 and Fig. 10 show the planar motion of the coupler and angular velocity of the coupler, respectively.

Table 1 Comparison of two other models

	Rigid body	RUML
Coordinates	4	4
Constraints	3	3
[B] Size	18×4	12×4
CPU times	5.63	5.17

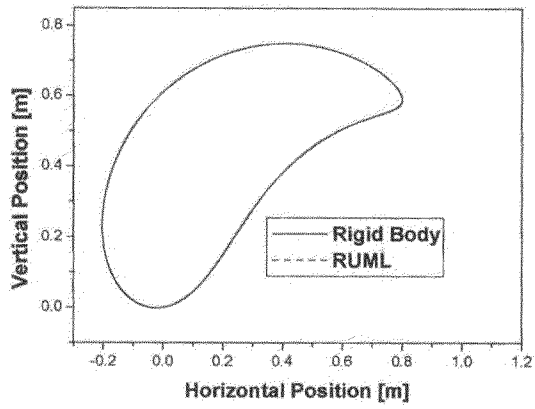

Fig. 9 Planar motion of the coupler

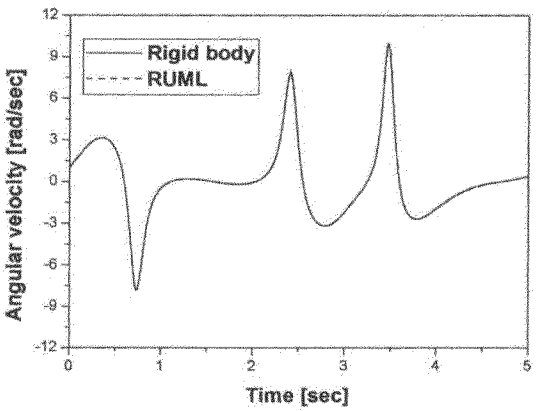

Fig. 10 Angular velocity of the coupler

Results of RUML model show good agreements with the rigid body model. The proposed model using the RUML shows the better efficiency than the rigid body model.

4.2 Vehicle Simulation

4.2.1 Vehicle Modeling

To confirm the new approach, a numerical simulation with a full vehicle model is performed.

Table 2 Properties of the vehicle system

Body frame	1046kg
Front suspension	Double-Wish bone type
Rear suspension	Solid axle with leaf spring
Tire	Full tire model
Steering system	Rack and pinion type
Total body number	15
Degree of freedom	15

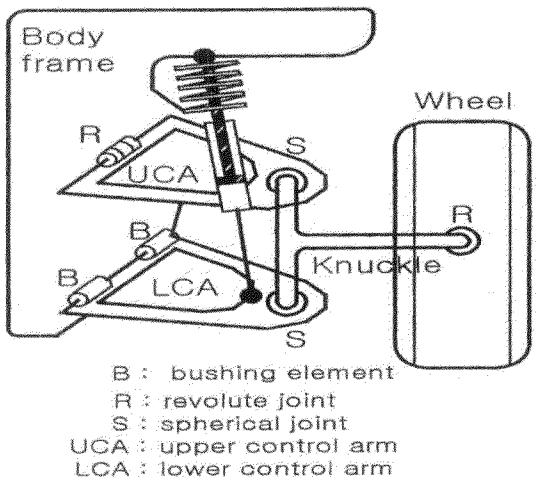

Fig. 11 Front suspension (Double-Wishbone suspension)

The front suspension of the vehicle shown in the Fig. 11 is a Double-Wishbone type. And a solid axle suspension with a leaf spring is installed in the rear wheels. The tire model used in simulation calculates the longitudinal, lateral, and vertical direction forces and moments. The steering system is a rack and pinion type. In the Fig. 12 and Fig. 13, rigid means a rigid body model and RSML represents massless link model. All the models contain a translational spring-damper on the lower control arm. The properties of the vehicle system are listed in Table 2.

4.2.1 Steering Simulation

When the vehicle is moving with a speed of 80km/hr, a half sine steering input is applied at the rackbar during 0. 3 second. Fig. 12 and Fig. 13 show yaw rate and lateral acceleration of the chassis frame, respectively. Two responses without bushing are almost identical. Two results with bushing are somewhat different from results without bushing due to bushing deformation.

Table 3 Comparison of CPU times in pulse steer simulation (SGI R10000 Octane workstation)

Case	Rigid w/o bushing	RSML w/o bushing	Rigid w/ bushing	RSML w/ bushing
Time [Seconds]	4.4	4.3	251.3	10.7

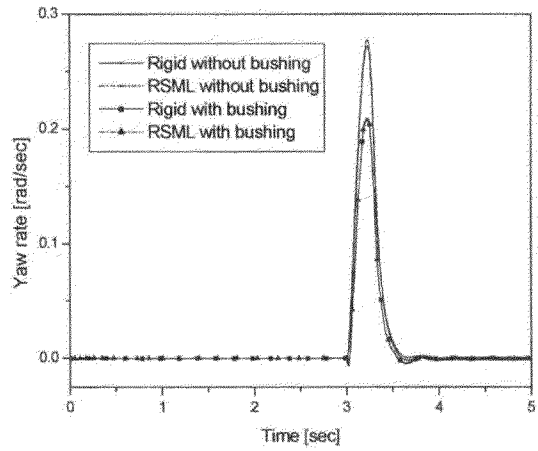

Fig. 12 Yaw rate of chassis frame

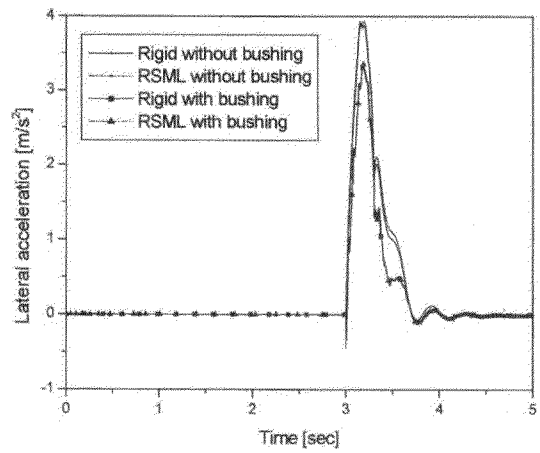

Fig. 13 Lateral acceleration of chassis frame

Table 3 shows the computational times of the four different models at the SGI workstation with R10000 chip. As shown in table 3, when there is no bushing, difference is not big between the rigid body model and a massless link model. However,

in case bushing is considered, computational times are quite different. RSML modeling technique including bushing elements is much more efficient than the conventional model.

5. Conclusions

In this paper, the velocity transformation matrix of massless links such as a revolute-spherical massless link and a revolute-universal massless link, which are useful in vehicle dynamics and modeling of a multibody system are formulated. In case generating the equations of motions by using the velocity transformation techniques, massless links can be modeled as the joints rather than the constraint equations through the new approach. Conventional modeling techniques such as a constraint model didnot handle a massless link transmitting force elements, which often appear in the lower control arm of McPherson or Double-Wishbone suspension. However, external forces applied on these massless links are resolved and transmitted to the neighboring bodies theoretically in this paper. The four-bar mechanism and the full vehicle system are tested to confirm the formulations of massless links. When the mass of a body is small and can be neglected, responses of a RSML model and RUML model are in a good agreement with a rigid body model.

When a bushing element is attached to a massless link model, a quasi-static formulation of bushing deformation enhances the numerical efficiency.

Acknowledgment

This research was supported by GRANT No. 97-0200-1001-5 from the KOSEF(Korean Science and Engineering Foundation)

References

Blundell, M. V., 1998, "The Influence of Rubber Bush Compliance on Vehicle Suspension Movement," *Materials and Design*, (19), pp. 29~37.

CADSI, 1995, *DADS Revision 8.0 User's Manual*, Oakdale, IA, U.S.A.

Haug, E. J., 1989, *Computer-Aided Kinematics and Dynamics of Mechanical Systems*, ALLYN AND BACON, Massachusetts, Volume I, pp. 69~71.

Kading, R. R. and Vanderploeg, M. J., 1985, *Dynamic Analysis of Vehicles Using a Rigid Body Dynamics General Purpose Computer Code*, Center for Computer Aided Design, The Univ. of Iowa, Iowa, Technical Report No. 85-6.

Kim, K. S. and Yoo, W. S., et al, 1999, "Development of Vehicle Dynamics Program AutoDyn7 (I)-Structure and Algorithm," *KSAE*, 7(3), pp. 321~330.

Kim, S. S. and Vanderploeg, M. J., 1986, "A General and Efficient Method Dynamic Analysis of Mechanical Systems using Velocity Transformations," *ASME Journal of Mechanisms, Transmissions, and Automation in Design*, 108(2), pp. 176~182.

Lee, B. H., Yoo, W. S. and Kwak, B. M., 1993, "A Systematic Formulation for Dynamics of Flexible Multibody Systems using Velocity Transformation Technique, " *I Mech E, J. of Mechanical Engineering Science*, Vol. 207 (C4), pp. 231~238.

M. D. I, 1994, *ADAMS Version 8.0 User's Guide, Ann Arbor*, MI, U.S.A.

McCullough, M. K. and Haug, E. J., 1986, "Dynamics of High Mobility Track Vehicles," *ASME Journal of Mechanism, Transmissions, and Automation in Design* (108), pp. 189~196.

Meirovitch, L., 1967, Analsys Methods in Vibrations, Macmillan Publishing, New York, pp. 30~37.

Nikravesh, P. E. and Gim, G., 1993, "Joint Coordinate Method for Analysis and Design of Multibody Systems : Part I. System equations," *KSME Journal*, 7(1), pp. 14~25.

Nikravesh, P. E., 1988, *Computer-Aided Analysis of Mechanical Systems*, Prentice-Hall, New Jersey, pp. 196~199.

Sohn, J. H. and Choi, S. T., et al, 2001, "Development of the Massless Link Model including External Force and Bushing Deformation," *KSAE*, 9(1), pp. 163~170.